Nuclear Magnetic Resonance Spectroscopy of Scandium in Perovskite Relaxor Ferroelectrics

A thesis submitted in partial fulfillment of the
requirement for the degree of Bachelor of Science in
Physics from the College of William and Mary in Virginia,

by

Mark W. Hibbard

Advisor:
Prof Gina L. Hoatson

May 2003

ABSTRACT

Scandium (^{45}Sc) NMR was used to explore the B-site order-disorder in the Perovskite piezoelectric material (1-x)$Pb(Mg_{1/3}Nb_{2/3})O_3$-x$Pb(Sc_{1/2}Nb_{1/2})O_3$ (PMN-PSN). The previously conducted experiments at higher magnet field strengths (9.4T and 14T) were supplemented by measurements at 7T and 3.5T. It was necessary to complete, repair, and calibrate the 3.5T spectrometer before experiments could be conducted on it.

INTRODUCTION **3**

THEORY **3**

NUCLEAR MAGNETIC RESONANCE 3

RELAXATION TIMES 6

PEROVSKITE RELAXOR FERROELECTRICS 3

NMR SPECTROSCOPY TECHNIQUES AND EQUIPMENT **8**

SIGNAL TO NOISE 8

MAGIC ANGLE SPINNING (MAS) 11

PREPARATORY WORK FOR ^{45}SC EXPERIMENTS: **12**

EXPERIMENT **14**

ANALYSIS 16

RESULTS AND DISCUSSION 18

Gaussian Decomposition – 7T *18*

Transverse Relaxation Time (T_2) Measurement *22*

Non-Results - 3.5T *25*

CONCLUSIONS **26**

INTRODUCTION

Peizoelectrics are a class of materials that undergo stress extension when current is passed through them and conversely generate a current when mechanically flexed. This unique property allows piezoelectric materials to be used as transducers, sensors, actuators, etc. Both PMN, PSN and their solid solutions are crystalline materials with particularly large electromechanical responses.[1] It is extremely important to understand their structure in order to formulate better and more effective piezoelectrics. Nuclear Magnetic Resonance Spectroscopy (NMR) is well suited to probing the structure of this disordered crystalline material. Once results are obtained using several different field strengths and temperatures, they can be analyzed to make inferences about structure and about the characteristic B-site order or disorder of the material, which is thought to be responsible for the relaxor ferroelectric behavior.

THEORY

Perovskite Relaxor Ferroelectrics

Perovskite relaxor ferroelectrics are a class of piezoelectrics. The relaxor behavior of PMN-PSN arises, in part, because of its disordered structure. The exact B-site order of the material is not fully understood. In order to further improve on these ferroelectrics, it is necessary to determine more precisely the B-site disorder and the displacements of cations from the crystalline structure and its effects on relaxor behavior.[1]

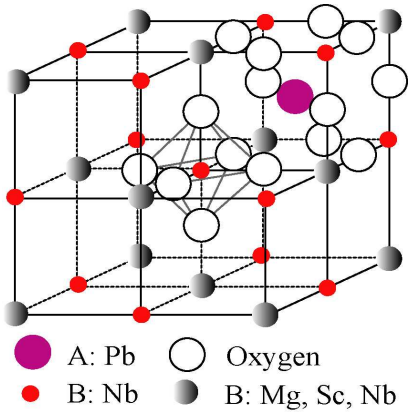

Figure 1 – PMN-PSN ideal perovskite unit cell[1]

It is hypothesized that the electromechanical response of PMN-PSN is largely due to local cation order and large-scale disorder. Particularly important is the order of the B-sites of the material. It was originally thought that the B-sites were populated randomly. Several experiments have ruled out this random ordering model, but have failed to fully describe the order that does exist[1]. ^{45}Sc NMR experiments on the quadrupolar interaction may be able to isolate any particular local structure surrounding the ^{45}Sc ions located at the B-sites in the PMN-PSN material, analogous to work done by Zhou, et al. on ^{93}Nb in PMN-PSN.[1]

Nuclear Magnetic Resonance

NMR spectroscopy is frequently used to investigate the structure of molecules and materials. The power of NMR lies in its ability to probe physical properties of materials in a nondestructive manner and over a wide variety of conditions (primarily temperature and state). Particularly important to this experiment is NMR's utility in determining the structure and dynamics in solid-state crystalline and amorphous materials.

In its most basic form NMR spectroscopy takes advantage of the magnetic properties of nuclei with non-zero angular momentum. By placing nuclei in a static magnetic field and irradiating them with a radio-frequency (RF) pulse it is possible to change their spin orientation. After the perturbation, the nuclei gradually return to their equilibrium state; during this "relaxation time", the nuclear spin vectors precess around the direction of the static magnetic field with certain discrete energies, depending on the spin orientation. This precession can be detected as an induced voltage in a RF coil placed perpendicular to the static field. By carefully selecting the energy (which is determined by

the frequency) of the incident RF radiation, recording the RF subsequently radiated by the nuclei, and analyzing the signals in both time and frequency space, it is possible to determine the characteristic spectrum of energy levels of the nuclei.[2]

Magnetic resonance of a nucleus is governed by several factors, the most important of which is the nuclear magnetic moment (μ), which is given by the following relationship:

$$\mu = \gamma I \hbar$$

where $\hbar$ is Plank's constant, γ is the proportionality constant (also called the magnetogyric ratio, a constant for each nucleus) and I is the total spin angular momentum of the nucleus.[3]

Spin angular momentum is essential to NMR. Classically, spin angular momentum can be conceptualized by imagining the nucleus spinning about its own axis. Quantum theory dictates, however, that angular momentum is quantized to certain values for the nuclei. These component spin quantum numbers result in specific allowed energy levels. In the absence of any magnetic field the energy levels are degenerate. However, in the presence of an external magnetic field (B_0), the energy levels separate according to the allowable orientations in the magnetic field. The energy of these different orientations is given by:

$$E = \gamma \hbar m_I B_0$$

where m_I is the component quantum number which describes the orientation of the spin with respect to the static magnetic field, and B_0 is the static magnetic field. For nuclei with total spin I, there are $2I+1$ possible orientations; therefore m_I can range from $-I$ to I in integer increments.[3]

For electromagnetic radiation induced excitations, spin orientations are restricted to transition between adjacent energy levels ($\Delta m_I = \pm 1$) . The RF pulse perturbs the precessing nuclei, forcing a jump to an adjacent energy level. After the application of the pulse, the nuclei eventually relax back to their equilibrium distribution of spin orientations. While the nuclei are in the perturbed states, they precess about the B_0 field at a certain frequency known as the Larmor frequency (υ_0), resulting in a changing magnetic field and thus an induced voltage in the RF pick-up coil. This frequency is determined by the difference between the two adjacent energy levels.[4]

$$\upsilon_0 = \frac{\gamma B_0}{2\pi}$$

To first order, these transition energies are all equal, so we would predict a delta function at the Larmor frequency in our Fourier transformed NMR signal (line-shape). However, other spin interactions also contribute to the shape and decay of the NMR signal, which allow insight into the molecular interactions and structure.

Relaxation Times

The nuclear relaxation back to the thermal equilibrium distribution is a product of several distinct relaxation mechanisms. The simplest of these is spin-lattice relaxation; the energized nuclei lose their energy to the surrounding crystal lattice by stimulated emission. This exponential relaxation is quantifiable and labeled T_1, the longitudinal relaxation time.

T_1 relaxation manifests itself in the NMR signal as a dampening parameter, resulting in a gradual decrease in amplitude of the signal. The exponential decay of the demodulated NMR signal is referred to as the Free Induction Decay (FID).[5] The spin-spin relaxation (T_2) is a catchall for the several causes of the broadening of a line-shape as well

as increasing the dampening of the Free Induction Decay. In practice, usually T_2 dominates T_1 in determining the FID decay time. One phenomenon that affects T_2 is the presence of slight inhomogeneities in the static magnetic field. These inhomogeneities shift the Larmor frequency slightly for different nuclei, depending on the exact local value of B_0. Immediately after the initial RF pulse, all the nuclei are precessing precisely in phase with one another. Due to slightly varied precession rates, they gradually begin to dephase, resulting in destructive interference of the magnetization vectors. This manifests itself in two different ways. First, the destructive interference increases the dampening of the observed FID. Second, due to the varying Larmor frequencies, there is a broadening effect on the theoretical delta function line-shape we predicted earlier.[4, 5]

Another factor contributing to the spin-spin relaxation time is the dipole-dipole coupling between nuclei. In a solid crystalline structure or a molecule (i.e. not just an isolated proton), the magnetic dipole of a nucleus causes significant changes to the magnetic moment of a neighboring nucleus. This variation is random with respect to the orientation of B_0, so it produces a random distribution of magnetic fields at the nucleus, and dephasing can occur between nuclei experiencing different local magnetic fields. In this manner, the dipole-dipole interactions also significantly broaden a line-shape, contributing to the observed spin-spin relaxation time, T_2.[4, 5]

Anisotropic chemical shifts can also result in line-shape broadening. Motion of nuclei and electrons create magnetic fields, which give rise to chemical shielding effects. When these occur in non-tetrahedral symmetry, the Larmor frequency for individual nuclei is shifted depending on its orientation and surrounding structure. These shifts affect the line-shape in a deterministic manner that can be isolated from other T_2 shifts. Specifically,

since the shifts are related to B_0, varying the magnetic field can determine how much of the broadening is due specifically to anisotropic chemical shifts.[2]

Of particular importance to the ^{45}Sc experiments is the electric quadrupolar interaction. Nuclei with total spin greater than ½ can have a nonspherically symmetric electric charge distribution, which interacts with electric field gradients (EFGs). These shift energies of the spin orientations. To first order approximation, the quadrupolar interaction shifts the -½ and +½ spins by the same factor, yielding no detectable difference. However, at second order we see a significant difference between these two energy levels. This results in a line-shape with peaks at characteristic frequencies, which can be analyzed to determine the EFGs and thus infer the crystalline or molecular structure.[2]

NMR Spectroscopy Techniques and Equipment

NMR spectroscopy is an excellent example of the inevitable interconnection between the disparate fields of theoretical physics and electrical engineering. While a thorough understanding of the physics of NMR is necessary in order to analyze the results of spectroscopy, the quality of the results is more a function of the design engineering and performance of the spectrometer. Many factors must be considered in order to extract high quality data from an NMR experiment.

Signal to Noise

By far, the most important consideration is that of signal-to-noise. Noise exists almost universally and there are many different varieties and sources of noise in any electrical system. Brownian motion of electrons in conductors induce random currents; interference from fluorescent lights or nearby college radio stations can cause unwanted

noise in signal lines; ironically, even the computers used to capture, store, and analyze NMR signals often operate at frequencies in the bandwidth of NMR signals. Further compounding the problem is the intrinsic low signal strength of the received NMR signal

The reason for this intrinsic low-level signal is of some significance to temperature dependent NMR experiments and worth a parenthetical aside. Higher absolute temperature results in more molecular motion. At absolute zero, there would be no molecular motion and all nuclear spins would line up parallel to B_0. However, with higher temperatures and thus more thermal energy, part of the population of nuclei arrange themselves anti-parallel to the magnetic field thus canceling the effects of the parallel aligned nuclei and results in a smaller net magnetization at equilibrium. The degree of this cancellation is related to the ratio of parallel to anti-parallel nuclei, known as the Boltzmann Distribution and largely determines intrinsic signal to noise ratio of the NMR signal.[4]

The key to these experiments is determining how to achieve an acceptable signal-to-noise ratio. There are the conventional methods for noise reduction employed by electrical engineers in all noise-prone systems: shielding, elimination of noise sources, careful grounding, and filtering. However, in NMR spectroscopy, an experiment can be repeated in a controlled and automated manner. By using a computer to trigger the generation of the RF pulse, control the timing, and record the results, the experiment can be automatically repeated an arbitrary number of times.

After repeating the experiment a number of times and summing the results (a process often termed coherent averaging) the scientist can take advantage of the random nature of noise. The signal of interest is coherent, i.e. it is roughly the same each time and will grow linearly with an increase in the repetitions of the experiment (or scans, denoted

by n). The noise, however, by its random nature will only grow as the square root of the number of scans. Therefore, the signal to noise ratio will be expected to grow as the square root of n:[4]

$$\left[\frac{S}{N}\right]_n = \sqrt{n}\left[\frac{S}{N}\right]_0$$

A problem arises with coherent-averaging, however. This is the problem of systematic distortion, offset, or noise addition to the NMR signal by the electronics used to demodulate, amplify, and digitize the signal. These artifacts would grow linearly as well, making them difficult or impossible to isolate from the signal. A common solution to this problem is phase cycling. Phase cycling takes advantage of the fact that the NMR signal is demodulated in order to place it in a frequency band that is easy to amplify and digitize. The demodulation yields a real and imaginary component (this is often called quadrature detection). The complex data point is then captured and digitized using two separate analog-to-digital conversion (ADC) channels. By cycling the phase of the incident RF pulse through 0°, 90°, 180°, and 270°, the phase of the NMR signal also goes through this rotation, causing the outputs to be swapped on imaginary and real channels, as well being inverted half the time. By cycling through each of these phases for a repeated experiment, the phase-shifted results can be corrected in software by a particular combination of swapping real and imaginary components and inversion. This has the effect of self-cancellation of the artifacts of distortion, offset, and systematic noise inherent in a particular electrical path between demodulation and digitization.[4]

In most NMR spectroscopy experiments (and ours in particular), the same coil is used to both radiate the RF pulse as well as to detect the resulting NMR signal (FID). A consequence of this is that both the high-powered RF amplifier and the high-gain, low-

power RF pre-amplifier are connected to the coil and, thus, to each other. All this interconnectedness, while elegant in its reuse of coils, connectors, and signal paths, is not without its dangers. In particular, there is the problem of high power RF pulses burning out the sensitive electronics in the pre-amplifier (which, in the case of this experiment has a gain of 75dB). A conventional work-around for this places a pair of cross-diodes at the input to the preamplifier. Diodes have a breakdown voltage of about 0.6V (essentially invisible to signals below this breakdown voltage, but short circuits to higher potentials), so the low-level NMR signal passes through unaffected, while the high power RF pulse is shunted to ground.[4] These cross diodes are typically placed at a cable length of $\lambda/4$ away from the T point in the path from the pulse amplifier to the probe. This enables a standing wave to form in the cable and keeps these cross-diodes from altering the impedance of the high power pulse at either the amplifier or the probe.

Further noise reductions techniques include the use of 100% shielded co-ax cable, the use of band-pass filters at the input and output of the RF amplifier to eliminate amplification of anything but the Larmor frequency of the spins.

Only after addressing these technical concerns can the scientist be confident in the results of the experiment. It is important to be conscientious of these considerations when conducting an experiment as well as when analyzing the results. Otherwise, erroneous conclusions may be drawn from noisy or uncalibrated data.

Magic Angle Spinning (MAS)

Another clever technique that is commonly employed in solid-state NMR spectroscopy is that of magic angle spinning (MAS). This is a trick that is used to narrow

the otherwise broad line-shapes of solid samples. Several factors contribute to line-shape broadening in solids, including dipole-dipole interactions and chemical shift anisotropies. Conveniently, the second-rank chemical shift anisotropy and dipole-dipole interaction have a factor of $(3\cos^2\theta - 1)$ in the Hamiltonian, where θ is the angle between the nuclear magnetization vector and the static magnetic field (B_0). We note that this factor goes to zero as θ approaches approximately 54.7° (the so-called "magic angle"). Rotating the sample rapidly around some axis z' effectively averages components of the nuclear magnetization vectors such that the net magnetization vector points only in the z' direction. So the sample is rotated about an axis, which is aligned at the magic angle with respect to the B_0 field. This causes all forms of the Hamiltonian containing the factor $(3\cos^2\theta - 1)$ to vanish, greatly reducing the line-width of solid-state spectra.

PREPARATORY WORK FOR ^{45}SC EXPERIMENTS:

The 150MHz (3.5T) spectrometer to be used in this experiment was not initially in a conveniently usable state. Several tasks were required to properly complete and calibrate the spectrometer before it can be used for ^{45}Sc experiments on the piezoelectric PMSN materials.

The transmitter, custom designed and constructed for this spectrometer by Vold and Wittebort (Figure 2) used digital data words loaded by digital control lines from the Libra data acquisition interface hardware, which was in turn controlled by the MacNMR©[6] software. The transmitter had sixteen volatile memory locations for phase words. The memory location used to determine the phase of the output of the RF pulse was selected via another data line from the Libra and could be switched using the MacNMR software.

The specific values for these words dictated the phase of the output RF pulse relative to the demodulated signal. It is imperative that we can accurately and reliably reproduce specific phases (most importantly: 0°, 90°, 180°, and 270°). The transmitter generated the output pulse in the following way: the demodulation frequency was phase shifted 90°. The phase shifted and original signals were mixed with amplitudes given by the phase words. This resulted in a signal of the same frequency, but an amplitude and phase shift given by the phase words in the following manner:

$$\sin\phi = \frac{I_y}{A}$$

$$\cos\phi = \frac{I_x}{A}$$

$$A = \sqrt{I_x^{\,2} + I_y^{\,2}}$$

where ϕ is the phase shift, I_x, I_y are the currents for the original and phase shifted signals, and A is the amplitude of the output.

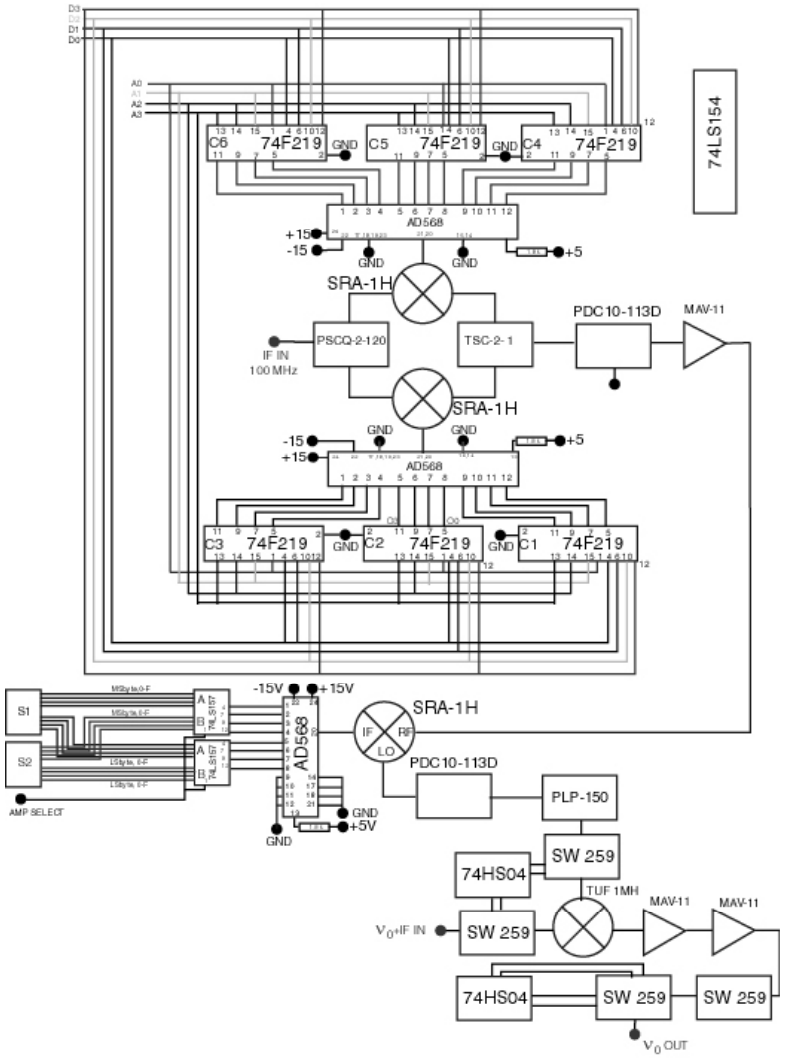

Figure 2 – Schematic of the transmitter custom designed by Vold and Wittebort. The 74F219 chips are volatile memory locations that determine the amplitudes of two signals oscillating at the intermediate frequency with a 90° relative phase relationship. These signals are mixed, determining the ouput phase and amplitude.

A heuristic technique was developed to assist in selecting phases and fine tuning the amplitudes. Several MacNMR sequences were developed, documented, and catalogued in order to aid in the future tuning of phase sequences. Careful measurements of phase and amplitude drift over the course of several weeks was also recorded and found to be acceptably within about 3% for a given power level. A phase table with data words for 0°, 90°, 180°, and 270° was then generated and saved to disk. On spectrometer power-up, this data table was loaded into the first four transmitter memory slots to allow for phase cycling.

Initial Deuteron experiments were conducted on a sample of heavy water to verify spectrometer functionality and ensure acceptable performance. This included construction of $\lambda/4$ cables and tuning of the Doty probe in order to have a characteristic impedance of 50 ohms and zero phase angle at the Deuteron Larmor frequency. Several bad cables, troublesome connections, and loaded power lines were detected and eliminated.

EXPERIMENT

To gain a better understanding of the role of ^{45}Sc in the order-disorder of the B-sites in PMSN two types of experiments were conducted and at two different field strengths. A magic angle spinning (MAS) echo experiment was conducted in order to attempt to resolve the different possible chemical configurations of nearest neighbors for the ^{45}Sc B-sites. This experiment was conducted at a field strength of 7T and compared with data previously collected at 7T[7], 9.4T[7] and 14T[7] for analysis.

Further, an experiment was conducted in order to measure the characteristic transverse relaxation time of PMSN (T_2). The data were analyzed to determine whether T_2

was constant across the frequency range of the characteristic second order quadrupolar ^{45}Sc spectrum.

The high-field experiments were conducted on an Oxford 7 Tesla cryomagnet and probe driven by an AMT pulse amplifier. The data acquisition equipment included Apollo Tecmag software and hardware, controlled by NTNMR software. The experiments took place at the College of William and Mary. The low field equipment included an 3.5 Tesla cryomagnet with a Doty Scientific probe and a CRC radio-frequency amplifier and other custom designed hardware (as described in previous section). The data acquisition hardware and software was a Libra Tecmag system. Custom written laboratory software DMFit[8], developed by Dominique Massiot was used for the deconvolution analysis.

Prior to each experiment, the probes were tuned to be purely resistive at 50 ohms (less than one degree phase). Preliminary experiments were conducted on a liquid $ScCl_3$ sample to shim the field (a process that involves tuning electromagnets in order to reduce inhomogeneities in the static magnetic field) and arrive at a reference value for the Larmor frequency in order to quantify any chemical shift observed in the solid sample. Cables were fabricated with lengths of appropriate ¼ multiples of the Larmor wavelength. Both 90° and 180° pulse lengths were determined by experimentally varying pulse length and searching for maximum and minimum FID envelopes.

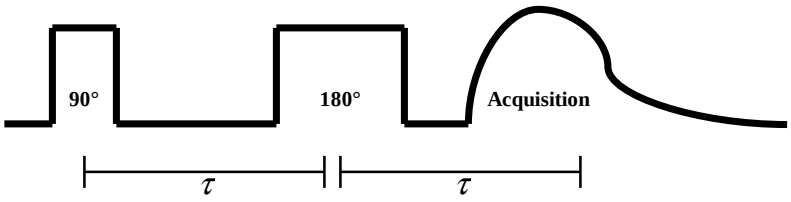

Figure 3 – Schematic of the MAS-echo pulse sequence. Acquisition began a fixed time after the 180° pulse and was left shifted in subsequent analysis in order to match time τ.

The MAS-echo experiments were conducted with a rotor spinning speed of 6 kHz at high field and a 2 kHz spinning speed at low field. The experiments consisted of a 90°-τ-180°-τ sequence with τ set to one period of the rotor spinning speed (Figure 3). Typical 90° pulse lengths were on the order of 3 μs and 5 μs for the 7T and 3.5T spectrometers, respectively. The magic angle of approximately 54.7° was tuned using a KBr solid sample.

The experiments used to obtain T_2 estimates were similar in nature to the MAS echo experiments. They consisted of a similar pulse sequence, but τ was varied in integer multiples of the rotor-spinning period (t_r, $2t_r$, $4t_r$, and $8t_r$). Data were left shifted to the top of the rotary echo for each sequence (an equal time τ after the 180° pulse) to accomplish proper phase alignment of the line-shape under Fourier transformation.

Analysis

The data were analyzed using NTNMR, DMFit, and MS Excel software. The NTNMR software was used to process the data into well-phased and clean Fourier transformed line-shapes. The DMFit software was used for constrained Gaussian deconvolution and graphing the line-shapes. Finally, MS Excel was used to calculate and graph the exponential regressions used to calculate T_2.

After an FID was collected experimentally, the data was baseline corrected to remove any DC offset in the signal. The data was then left shifted an appropriate number of points in order to align the phase correctly. The number of left shift points was analytically determined to match the effective delay time (the sum of the actual delay time to acquisition and the equivalent delay time of left-shit points) after the 180° pulse to the

time τ (between the 90° and 180° pulses). The FID was anterior zero-filled to allow for more interpolated points in the subsequent Fourier transform. The data was then complex Fourier transformed. Zeroth and first order phase correction was applied to the line-shape in order to maximize symmetry and minimize the baseline. Lastly, the data was exported to a tab delimited ASCII file.

The DMFit software was employed to calculate the Gaussian decomposition of the MAS echo experimental data. The line-shape was loaded into the software and initial parameters were selected for one, two, three, and four Gaussian components. An iterative best-fit routine was run until convergence and the final fit results were recorded.

In order to calculate T_2 robustly, amplitude data were taken at three different frequency points on each of the four line-shapes. These frequencies roughly corresponded to the peak and the two half-height points. The natural log was taken of these three exponential decay data sets and a linear regression was performed to arrive at a measurement for T_2. The R^2 values for the linear regression fits were also recorded.

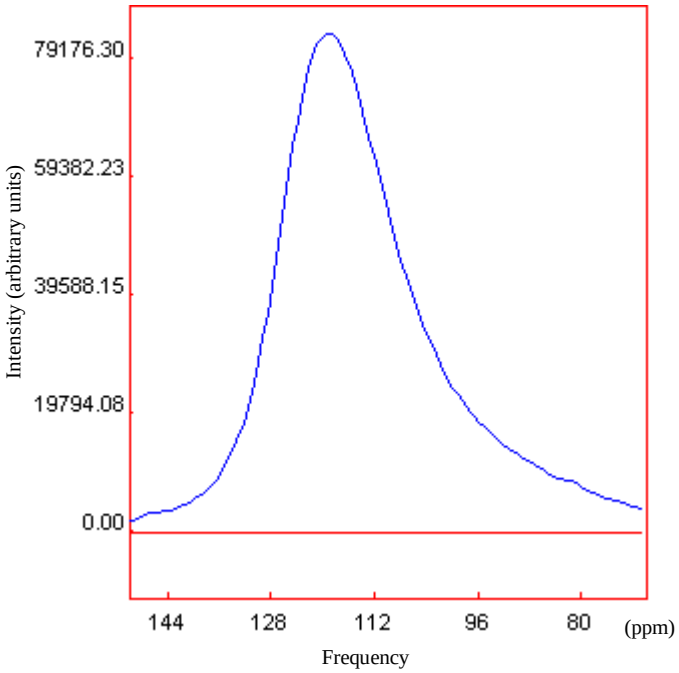

Figure 4 – PMSN (x=0.7) MAS spectrum taken at 7T using a MAS-echo pulse sequence. Data has been baseline corrected and phase adjusted. Reference frequency was 79.89063MHz

using the DMFit software. A careful examination of the line-shape reveals an asymmetry (Figure 4), which belies the possibility of multiple quadrupole coupling constants due to certain allowed configurations for the nearest neighbors of ^{45}Sc populating the B-sites. The number, nature, and relative distribution of these configurations in the PMSN (x=0.7) sample is unknown. However deconvolution allows us to gain qualitative

Results and Discussion

Gaussian Decomposition – 7T

A high-scan-number (n=10000) experiment on the 7T magnet yielded low-noise data, which was deconvoluted

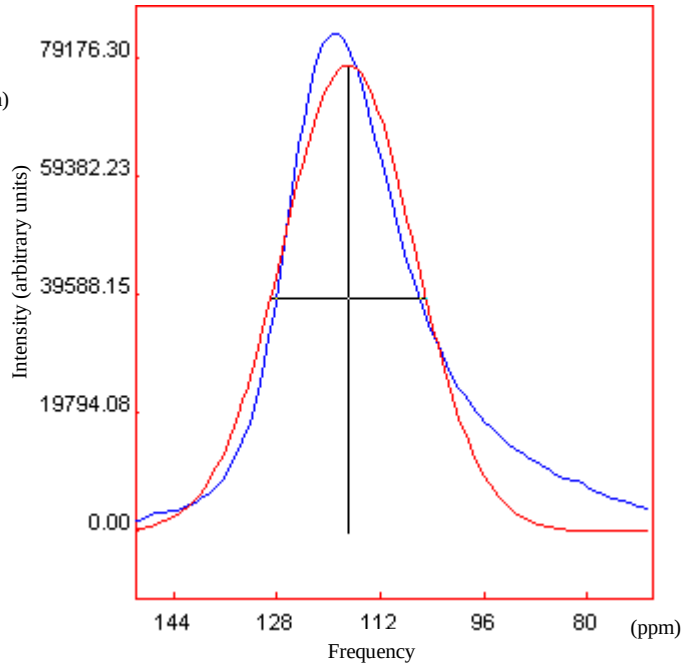

Figure 5 – PMSN (x=0.7) MAS spectrum taken at 7T using a MAS-echo pulse sequence. Data has been baseline corrected and phase adjusted. A single Gaussian deconvolution of the data has been superimposed.

Table 1 – One Guassian Deconvolution

	Parameters		
	Amplitude (arb. units)	Location (ppm)	Width (ppm)
1	77856.22	117	24.09
Sdev	6286.503		

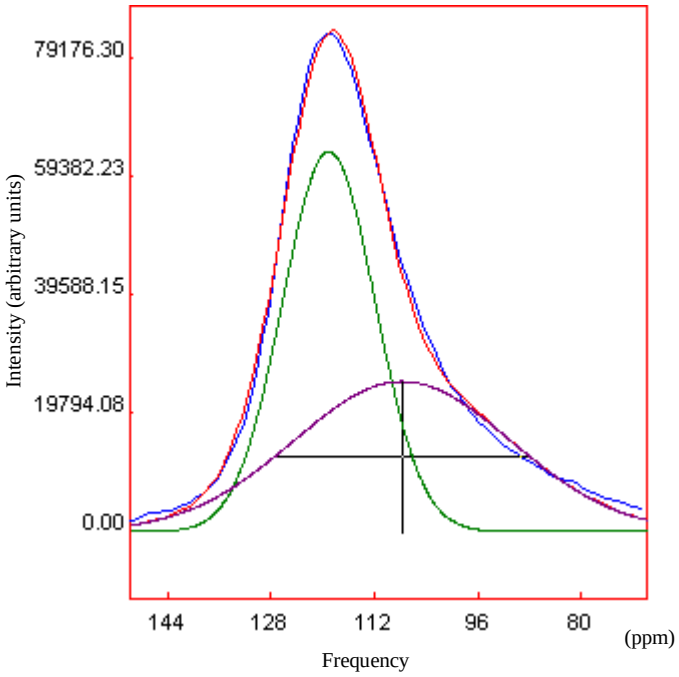

Figure 6 – PMSN (x=0.7) MAS spectrum taken at 7T using a MAS-echo pulse sequence. Data has been baseline corrected and phase adjusted. A double Gaussian deconvolution of the data has been superimposed with the following parameters:

Table 2 – Two Gaussian Deconvolution – 7T

Parameters			
	Amplitude (arb. units)	Location (ppm)	Width (ppm)
1	63427.14	119.08	16.87
2	2506.05	107.73	39.4
Sdev	1333.278		

insight into the possible configurations and their populations.

Further illustrating the high likelihood of multiple (at least two) possible nearest neighbor configurations for ^{45}Sc is the poor fit of a single Gaussian deconvolution (Figure 5). The poor standard deviation (Sdev=6287) of the fit parameters highlights the asymmetries of the experimental line-shape. Although not perfect, a much better fit (Sdev=1333) is achieved with two Gaussians (Figure 6).

It is worth noting that all parameters (amplitude, width, and location) were allowed to vary for all Gaussians. Without any constraints, increasing the number of Gaussians will inevitably allow for a better fit, but not necessarily be physically justified. As such, a convincing argument can only be made that ^{45}Sc in PMSN (x=0.7) has at least two chemical B-site configurations. Further quantitative analysis (i.e. the exact number and make-up of chemical configurations as well as their relative distribution in the material) is extremely difficult without a more resolved spectrum.

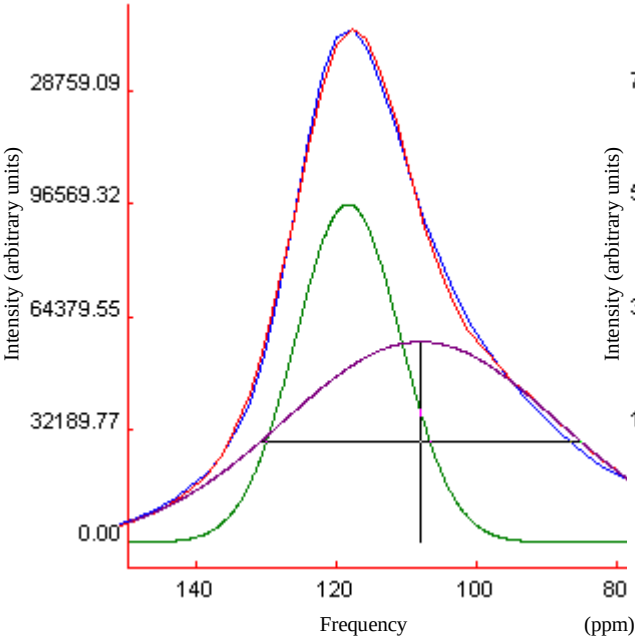

Figure 7 – PMSN (x=0.7) MAS spectrum taken at 9.3T using a MAS-echo pulse sequence[7]. Data has been baseline corrected and phase adjusted. A double Gaussian deconvolution of the data has been superimposed with the following parameters:

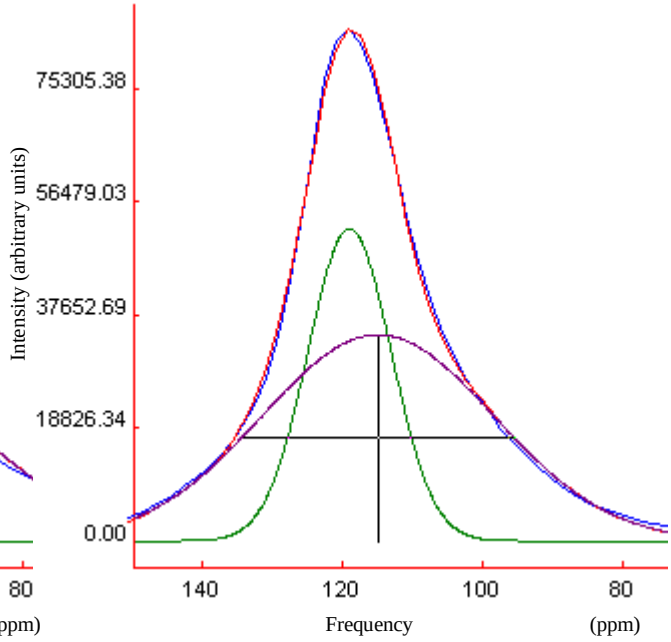

Figure 8 – PMSN (x=0.7) MAS spectrum taken at 14T using a MAS-echo pulse sequence[7]. Data has been baseline corrected and phase adjusted. A double Gaussian deconvolution of the data has been superimposed with the following parameters:

Table 3 – Two Gaussian Deconvolution – 9.4T

	Parameters		
	Amplitude (arb. units)	Location (ppm)	Width (ppm)
1	96312.79	118.46	17.65
2	57150.20	108.13	45.87
Sdev	868		

Table 4 – Two Gaussian Deconvolution – 14T

	Parameters		
	Amplitude (arb. units)	Location (ppm)	Width (ppm)
1	52008.54	119.15	14.00
2	34342.01	115.08	38.89
Sdev	1337		

There was a hope that performing NMR at lower fields would result in a higher resolution for the different nearest neighbor configurations. This would be the case if the primary factor in the non-degeneracy of the different B-site configurations was due to the quadrupolar interaction while the half-height full-width of the individual configurations was due mainly to a distribution of chemical shifts (or possibly dipolar interactions not cancelled by MAS). The magnitude of dipole-dipole interactions is independent of field strength, and the chemical shift distribution would scale linearly with field strength,

reducing the component line-width at lower fields. However, the quadrupolar interactions would scale inversely with field strength, enhancing the separation of the B-site configurations, and thus improving resolution.

$$X = \frac{ax_q}{\lambda_L} + bx_{cs}\lambda_L + cx_d$$

A qualitative comparison of the relative resolution of the previously collected data at high fields (9.3T and 14T, see Figures 7 and 8) and the data collected at the lower 7T field strength (Figure 6) shows this hope to be unfounded. On visual inspection, it appears that the width of the possible individual B-site configurations as well as the width of the

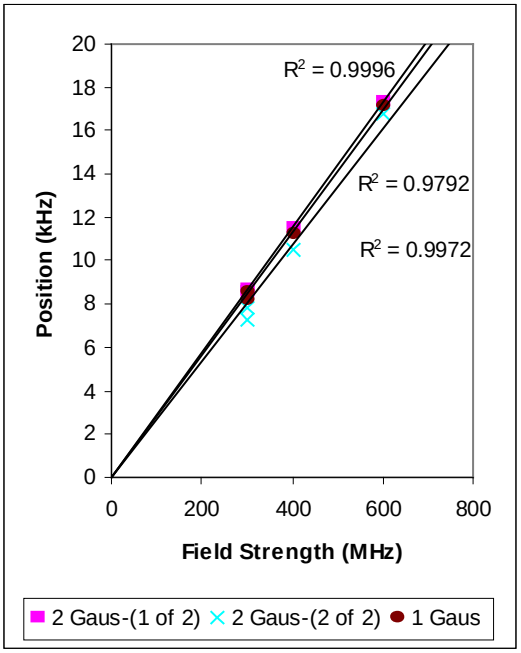

Figure 9 – A plot of the location of the deconvolved Gaussians as a function of field strength. Both single and double Gaussian deconvolutions are plotted. A linear regression (constraint: b=0) for each data set is superimposed. The high correlation denotes the isotropic chemical shift as the dominant interaction for determining the separation and location of the different B-sites.

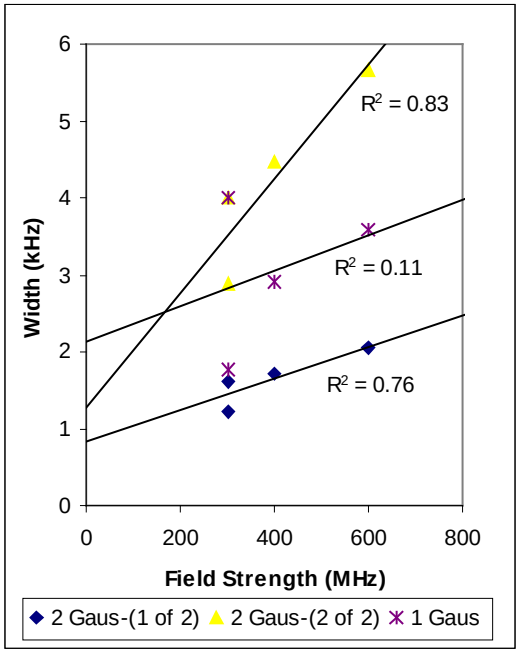

Figure 10 - A plot of the width of the deconvolved Gaussians as a function of field strength. Both single and double Gaussian deconvolutions are plotted. A linear regression is plotted for each data set, although the correlation is low. Within experimental error, it is hard to make conclusive inferences as to the exact nature of the relationship between field strength and deconvolved Gaussian width.

overall line-shape both scale linearly with field strength. By plotting the deconvolved Gaussian parameters against field strength (Figures 9 and 10) we can make further inferences about the mechanisms responsible for the B-site line-shape interactions and distributions. Figure 9 gives good evidence for Gaussian location being related to field strength by some linear factor. Figure 10 is not as conclusive, but it appears as though there is a positive correlation between field strength and Gaussian width. In any case, the quadrupolar interaction, which would scale *inversely* with field strength, does not appear to be the dominant interaction. Neither does the dipole-dipole interaction appear to be very large, which would be constant across all field strengths. Rather, the highly linear relationship between Gaussian position and field strength is convincing evidence for a distribution of isotropic chemical shifts dominating. Therefore, conducting the NMR experiments at lower field strengths does not appear to promise additional spectral resolution as previously hoped. It does, however, help to unambiguously identify the origin of the broadening mechanism.

Transverse Relaxation Time (T_2) Measurement

Multiple lower-scan-number (n=2048) experiments were conducted, varying the time τ in the echo sequence to determine the exponential decay of the NMR signal due to transverse relaxation modes (from spin-spin coupling: dipole-dipole coupling and chemical shift anisotropies, among others). If the different B-site configurations had dissimilar transverse relaxation times because of varying spin-spin couplings among the configurations, T_2 measurements would yield different results at different points on the spectrum. This would be good evidence that the asymmetrical nature of the ^{45}Sc line-shape was due primarily to specific non-random disordered B-site configurations.

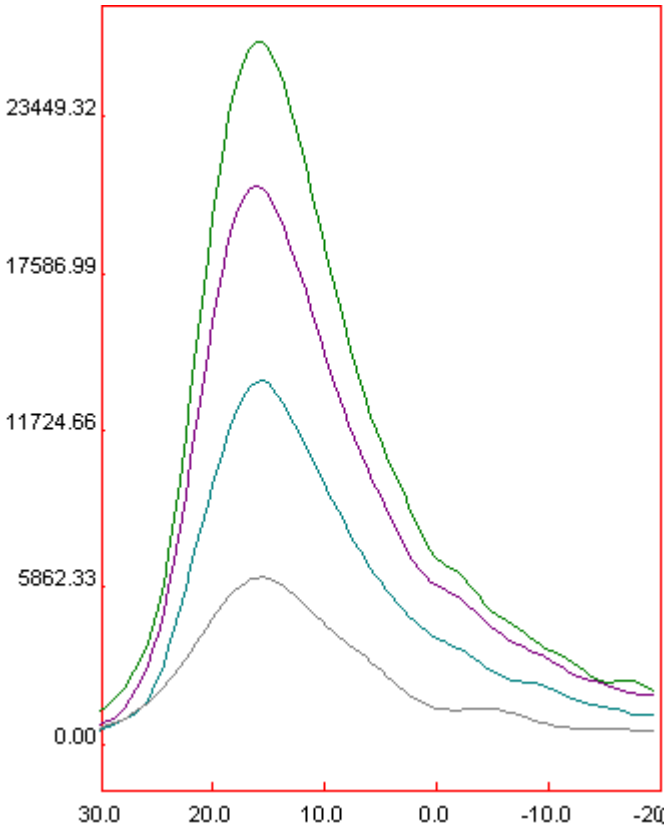

Figure 11 – Stacked plot of PMSN (x=0.7) MAS echo spectra with τ at 0.166ms, 0.332ms, 0.664ms, and 1.328ms (effectively measuring T_2 decay rate), with a reference frequency of 72.89766MHz.. Notice the similar shape of all four spectrum, signaling a similar T_2 for all B-site configurations present in the material.

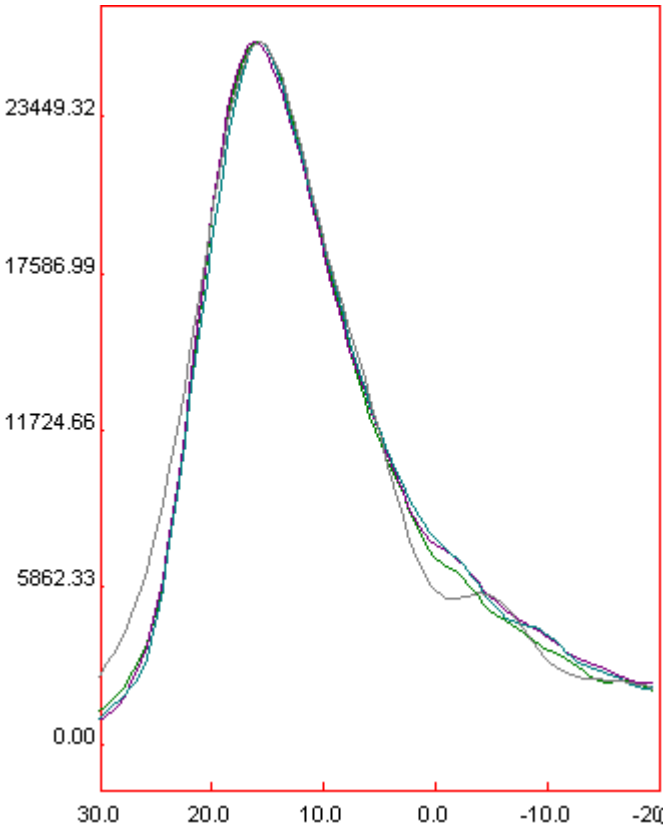

Figure 12 – Stacked plot of PMSN (x=0.7) MAS echo spectra with τ at 0.166ms, 0.332ms, 0.664ms, and 1.328ms with a reference frequency of 72.89766MHz. These have been normalized for an easier qualitative comparison of line-shape. There is a slight divergence near 0ppm, which is evidence for a unique B-site at that location.

The initial results indicated that T_2 is constant for three points across the line-shape (within the experimental error). This can be seen qualitatively in Figures 11 and 12. If T_2 varied with frequency, the shape of the MAS spectrum would vary with time τ. As seen in Figure 10, all four experiments yielded similar shapes for the ^{45}Sc spectrum. More quantitatively, T_2 was initially measured at 3 chosen frequencies (0.68 kHz, 1.61 kHz, and 2.20 kHz; chosen because they were the locations of the peak and the two half-height points on the initial spectrum) by performing a linear regression on the natural log of the amplitudes. One can see the equivalent exponential fit on the graph in Figure 13. The

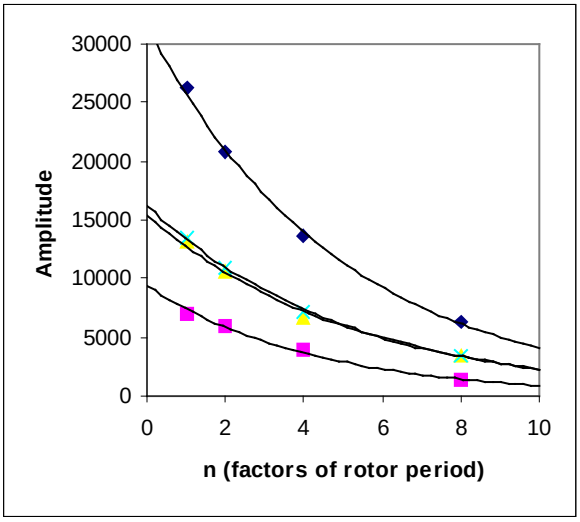

Figure 13 – The exponential decay function (with time constant T_2) of three locations on the PMSN (x=0.7) spectra. Squares correspond to data points measured at the 0 kHz, diamonds at the 0.682 kHz location, x's at 1.61 kHz and triangles at 2.196 kHz. An exponential best fit regression has been superimposed for each series.

Freq (kHz)	**T_2** (ms)	**+/-**
0.010	1.40	0.09
0.682	1.69	0.04
1.610	1.63	0.04
2.196	1.75	0.11
Mean	1.62	

Table 5 – T_2 measurements for three locations on the PMSN (x=0.7) spectra. The locations were taken as the peak, the two half-height points, and 0ppm.

initial results of the T_2 measurements yielded approximately 1.7 ±0.1 ms for all three locations.

However, closer inspection of the line-shape in the region from 0 to –10.0 ppm reveals that the relative intensity varies with time τ (best seen in Figure 12). This prompted further analysis and the 0ppm point was added to the three initial points (Table 5). A T_2 estimate of this point yielded 1.4 ±0.1 ms, a significant difference from the other three points. This is good evidence of different B-site configurations contributing to the overall line-shape. It is worth noting that none of the peaks of the Gaussians in the two Gaussian deconvolution corresponded to this 0ppm point. However, it is quite possible that more Gaussians are required to adequately model this line-shape. Additional Gaussians in the deconvolution might have yielded one with its peak at the 0ppm point.

Non-Results - 3.5T

The observant reader will notice the absence of any 3.5T results in the previous two sections of results discussion. After all, much of the preparatory work went into the construction and completion of the 3.5T spectrometer. The reason for the exclusion of low-field results is the lack of low-field results at the time of this writing. The 3.5T spectrometer was in working order and yielded nominal results for the benchmark $ScCl_3$ sample, but failed to return any discernable signal for solid samples.

Numerous explanations can be proffered for the absence of a solid-state signal. Primary among them is the inherent low signal to noise ratio of a solid-state signal. Contributing to this is the large width of the line-shape of solids, resulting in a fast decay of the FID. Since a requisite delay time must be added between pulsing and acquisition to allow the pre-amplifier electronics to recover, much of the signal has already decayed by the time acquisition has begun. In addition, the lower field strength results in an inherently smaller signal to noise ratio, since the Boltzmann population distribution is smaller at the lower field strength.

At the time of this writing, it appears that this inherent small signal strength of the solid state sample was ill-matched to the first stage of gain in the pre-amplifier (i.e. the gain was too small). Increasing that gain appears to result in a measurable solid-state signal. Regardless, as the analysis of the 7T results indicates, the possible advantage of performing experiments at low field (improved resolution of primarily quadrupolar interaction separated B-site configurations) was not manifested and the disadvantages (lower signal to noise ratio) are still present. These considerations make the 3.5T results less crucial than previously anticipated.

CONCLUSIONS

^{45}Sc results from the 7T spectrometer on the PMSN (x=0.7) ferroelectric material sample yielded several interesting discoveries. A qualitative comparison of deconvolution and central transition line-shape broadening between 7T, 9.4T, and 14T reveals that lower field strengths do not improve the resolution of different B-site configurations for the ^{45}Sc. One possible explanation for this is that the interactions contributing to the separation of B-site configurations also contributes to the width of each B-site configuration distribution. In other words, the each B-site configuration has some distribution of interactions, which also scales similarly with reduced field strength. Furthermore, the line-shape separation scales roughly linearly with field strength, which amounts to strong evidence for a distribution of isotropic chemical shifts dominating over the second order quadrupolar or dipole-dipole interactions. The asymmetry of the line-shape points to some distribution of configurations, but the lack of resolution makes it difficult to discern with any certainty what these configurations are and what their relative population densities are.

Measurements of T_2 across several frequencies demonstrated that there was a measurable difference in the transverse relaxation time at the 0ppm point compared to the rest of the line-shape. This is evidence that the ^{45}Sc line-shape is a result of several different B-site configurations with different transverse relaxation times.

Finally, significant progress was made on the construction and completion of the 3.5T spectrometer. Although more bugs may still have to be worked out, it appears to be functional and ready for one-channel MAS NMR experiments on ^{45}Sc (and other nuclei). A second transmitter channel has been added and calibrated. A second set of cables, pre-amp, cross-diode networks, and demodulator must be added to conduct two-channel

experiments. Work still remains on completing and testing temperature control for use in variable temperature experiments as well as increasing the maximum rotation speed for MAS. Currently, the spinning hardware is only capable of spinning consistently and stably at about 2 to 3 kHz.

---

[1] G. L. Hoatson, D. H. Zhou, F. Fayon, D. Massiot, R. L. Vold, Phys. Rev. B **66**, 224103 (2002)

[2] J.W. Akitt, *NMR and Chemistry: An introduction to modern NMR spectroscopy* (Chapman & Hall, London, 1992), pp. 11, 95, 85-91

[3] R.J. Abraham, J. Fisher, and P. Loftus, *Introduction to NMR Spectroscopy* (John Wily and Sons, Chichester, 1988), pp. 2

[4] E. Fukushima, S. B. W. Roeder, *Experimental Pulse NMR: A Nuts and Bolts Approach* (Addison-Wesley Pub. Co., Reading, MA, 1981), pp. 4, 130-132, 6, 437, 60-75

[5] C. Dybowski, R. L. Lichter, *NMR Spectroscopy Techniques* (Marcel Dekker, Inc, New York, 1987, Vol 5), pp. 46-72

[6] **MacNMR** © 2002, by TecMAG, Inc.

[7] Data collected by Dr G.L Hoatson

[8] "dmfit program" : D.Massiot, F.Fayon, M.Capron, I.King, S.Le Calvé, B.Alonso, J-O.Durand, B.Bujoli, Z.Gan, G.Hoatson, "Modelling one and two-dimensional Solid State NMR spectra.", Magnetic Resonance in Chemistry, **40** 70-76 (2002).